Nat. Hazards Earth Syst. Sci. Discuss., 2, 1405–1431, 2014
www.nat-hazards-earth-syst-sci-discuss.net/2/1405/2014/
doi:10.5194/nhessd-2-1405-2014

Natural Hazards and Earth System Sciences
Open Access
Discussions

Soil erosion in an avalanche release site (Valle d'Aosta: Italy): towards a winter factor for RUSLE in the Alps

S. Stanchi[1,2], M. Freppaz[1,2], E. Ceaglio[3], M. Maggioni[1,2], K. Meusburger[4], C. Alewell[4], and E. Zanini[1,2]

[1]Department of Agriculture, University of Torino, Forest and Food Sciences (AGRIFORFOOD), Via L. Da Vinci 44, Grugliasco, TO 10095, Italy
[2]University of Torino, NATRISK, Research Centre on Natural Risks in Mountain and Hilly Environments, Via L. Da Vinci 44, Grugliasco, TO 10095, Italy
[3]Fondazione Montagna Sicura – Montagne Sûre, Villa Cameron, Località Villard de la Palud, 1, 11013 Courmayeur (AO), Italy
[4]Institute of Environmental Geosciences, University of Basel, Bernoullistr. 30, 4056 Basel, Switzerland

Received: 27 November 2013 – Accepted: 17 January 2014 – Published: 11 February 2014

Correspondence to: S. Stanchi (silvia.stanchi@unito.it)

Published by Copernicus Publications on behalf of the European Geosciences Union.

Abstract

Soil erosion is largely affecting Alpine areas. In this work we compared ^{137}Cs-based measurement of soil redistribution and soil loss estimated with RUSLE in a mountain slope affected by full depth snow-glide avalanches, in order to assess the relative importance of winter erosion processes through a correction factor (*W* – winter factor). Three subareas were considered: SB, snow bridge areas; RA, release area, and TA, track area, characterized by different prevalent winter processes.

The RUSLE estimates and the ^{137}Cs redistribution gave significantly different results (higher for ^{137}Cs method), confirming a relevant role of winter erosion.

W ranges evidenced relevant differences in the role of winter erosion in the considered subareas, and the application of an avalanche simulation model corroborated these findings.

Despite the limited sample size (11 points) the inclusion of a *W* factor into RUSLE seems promising for the improvement of soil erosion estimates in Alpine environments affected by snow movements.

1 Introduction

Soil erosion hazard is largely affecting mountain areas (JRC, 2009a, b). While the causes and effects of erosion as a soil degradation threat in the world are widely described and investigated (Lal, 2001), the soil loss estimation in sloping areas still has some uncertainties, as the methods commonly used are not specifically designed for mountain environments, where climate and relief are extreme (Alewell et al., 2008). Recently, the relevance of winter erosion processes, besides the ones taking place in the growing season, has been pointed out. Konz et al. (2009) suggested the development of an "Alpine USLE" including an Alpine factor *W* implemented for slopes that are prone to avalanches and snow gliding processes. Ceaglio et al. (2012) proved that snow movements are a significant agent of soil redistribution in mountain sites.

NHESSD
2, 1405–1431, 2014

Finally, Konz et al. (2012) in a study on the methods to measure soil erosion in the field concluded that snow-driven processes are dominating in Alpine grasslands.

One of the most commonly applied methods for soil erosion estimation is the Revised Universal Soil Loss Equation (RUSLE) derived from USLE (Wischmeier and Smith, 1978), which has received considerable improvements after the introduction of Geographic Information Systems (Desmet and Govers, 1996; Prasuhn et al., 2013; Zhang et al., 2013). The erosion rate derived from RUSLE corresponds to water erosion and cannot consider snow-induced erosion. According to the USLE procedure, snowmelt can be included in the erosivity factor by multiplying the precipitation falling in the form of snow by 1.5 and then adding the product to the kinetic energy times maximum 30 min intensity. However, the heterogeneous redistribution of snow by drifting, sublimation, and reduced sediment concentrations in snowmelt confuses the problem tremendously (Renard et al., 1997). Consequently, RUSLE estimates for mountain areas often show significant deviations from field-measured data obtained during the growing season on snow-free soil (Konz et al., 2009). This common finding suggests that more complex phenomena are driving soil erosion in mountain environment and that erosion in areas seasonally snow covered might be affected considerably by other agents of erosion (Confortola et al., 2012), such as snow avalanche, characterized by high velocity, and snow gliding, the slow downhill movement of the snow cover on smooth and/or wet ground.

Besides sediment collection, another method to derive erosion rates from field measurements are fallout radionuclides like Caesium-137 (^{137}Cs). ^{137}Cs is an anthropogenic isotope that originated from the testing of thermonuclear weapons and the Chernobyl accident. When ^{137}Cs fallout reaches the soil surface, it is tightly adsorbed to fine soil particles (Tamura, 1964; Tamura and Jacobs, 1960). Thus, its subsequent redistribution is associated with soil redistribution (Ritchie and McHenry, 1990). The ^{137}Cs method has the major advantage to reflect all erosion processes by water, snow and wind and is thus an integrated estimate of the total net soil redistribution rate since the 1950s (the start of the global fallout deposit) and since 1986 (in areas where the

NHESSD
2, 1405–1431, 2014

major fallout originated from the Chernobyl accident). Fallout radionuclides are therefore largely used to assess the budget of soil erosion and sedimentation processes (Mabit et al., 2008, 2013; Mabit and Bernard, 2007; Matisoff and Whiting, 2011).

Due to the different soil erosion processes and time scales considered, also ^{137}Cs soil erosion estimates are often not directly comparable with RUSLE estimates. In mountain areas the deviations between RUSLE and available measurements have been commonly attributed to an intrinsic unsuitability of the model for steep and complex topography, but they might depend also on the presence of relevant snow-driven erosion phenomena that are not included in the rainfall erosivity factor (R) of RUSLE (Konz et al., 2009).

The potential phenomena that could generate erosion on snow covered slopes are avalanches and snow gliding. Flowing avalanches can produce considerable soil removal and sediment transport both in the release and track zones (Confortola et al., 2012), altering the soil morphology at the local scale, transporting a significant amount of soil across the runout zone (Freppaz et al., 2010; Ceaglio et al., 2012). If full-depth avalanches predominate, and the avalanche flows interact directly with bare ground, then soils could be stripped off in the track zone and could be fragmented and/or highly degraded (Freppaz et al., 2006, 2010). Complex soil profile morphologies may occur along an avalanche path with both buried and truncated horizons. In addition, snow gliding phenomena can contribute significantly to soil erosion at the snow/soil interface. The sediment properties and composition vary depending on the magnitude and frequency of disturbance (Freppaz et al., 2006). Soil removal from avalanches has been modeled and quantified by Confortola et al. (2012), who compared the critical soil stress with the shear stress exerted by the avalanche, concluding that soil erosion due to avalanches occurs almost everywhere along an avalanche path. Snow gliding has been investigated and modeled by Leitinger et al. (2008).

The inclusion of a correction factor accounting for winter erosion processes (Winter factor, W) into RUSLE has been proposed by Konz et al. (2009), who observed a significant deviation between measured and estimated soil loss on different vegeta-

NHESSD
2, 1405–1431, 2014

tion types, suggesting for the first time the presence of different forces driving winter erosion. However, the incidence of snow-induced erosion at large scales (e.g. catchment or avalanche areas) may show considerable spatial variation and is therefore very difficult to quantify. However, in some cases the predominance of the snow-related phenomena in soil erosion is undoubtable, as reported for example by Ceaglio et al. (2012) in the Italian Alps, who compared field measured and ^{137}Cs derived soil redistribution rates.

Starting from these results, the general aim of the present research is to compare ^{137}Cs-based measurement of soil redistribution and soil loss estimated with the RUSLE model in a mountain slope affected by full depth snow-glide avalanches. We will investigate eleven sites distributed along the different areas of a snow avalanche path: the release area (RA), where avalanche release and slow snow cover movements take place; the track area (TA) directly affected by the avalanche run and a third area, protected by snow bridges (SB) that are designed to reduce snow cover movements, where avalanche release is excluded but slow snow cover movements can still occur. The specific objectives are: (1) to apply the GIS-based RUSLE in a mountain site affected by recurrent glide-snow avalanches; (2) to compare the soil erosion estimates obtained from the application of the RUSLE with the ^{137}Cs budget estimated from a previous field survey carried out by Ceaglio et al. (2012); (3) to test a winter correction factor (W) for RUSLE referring to winter soil erosion contribution; (4) to discuss and interpret the results considering a 2-D avalanche dynamic model.

2 Materials and methods

2.1 Study area

The study area is an avalanche site named Mont de la Saxe located in the northwestern part of the Valle d'Aosta Region (NW-Italy, Fig. 1a), very close to the south side of the Mont Blanc Massif (4810 m a.s.l.). The avalanche site (24.6 ha, Fig. 1b)

NHESSD
2, 1405–1431, 2014

ranges from 2115 m to 1250 m a.s.l. Three subareas were considered (RA, release area; TA, track area; SB, snow bridge area), where 11 sampling points were chosen. While choosing sample points for this study, areas affected by complete topsoil removal were excluded.

The geology is characterised by black argillic schists, calcareous sandstones and a limited portion of porphyritic granites, very similar to that characterizing the Mont Blanc area. The site is affected by glide-snow avalanches occurring in spring time or late autumn, and is prone to snow gliding and subsequent glide cracks formation. Soil erosion is very pronounced and clearly related to snow–soil interface dynamics (Ceaglio et al., 2012), as soil is frequently removed by avalanches and large soil deposits can be observed in the runout area. In the last four years, glide-snow avalanches were documented almost yearly (Ceaglio et al., 2014). Most of the area is Alpine pasture, with patches of dwarf shrubs. The avalanche release area (RA) is located at 2100 m a.s.l. (steepness 30–35°), and covered by abandoned pasture. Snow bridges (SB) are present close to this sector, on similar slopes, and the protected surface is colonized by dwarf shrubs and larch seedlings. The track area (TA) ranges from 2000 and 1350 m a.s.l. and is characterized by the presence of different channels, with grass cover or bare soil and rock outcrops in the steepest sections. The runout area starts at 1200 m a.s.l., ends on an avalanche shed and is characterised by decreasing steepness. An exhaustive description of the avalanche site and dynamics, as well as the sampling strategy in the area, is provided by Ceaglio et al. (2012).

2.2 Soil properties

In general, soils in the study area are shallow and scarcely developed.

The upper soil horizons had a sand content ranging from 32 to 60 %, and a clay content ranging from 6 to 20 % (Ceaglio et al., 2012). The soil bulk density ranged between 659 kg m^{-3} (SB) and 1073 kg m^{-3} (RA), and the skeleton content from 5 to 44 % (Ceaglio et al., 2012). The organic carbon content (data not shown) was higher in SB (4.9 %) and lower in RA (3.3 %) and TA (3.8 %), suggesting an enrichment of

NHESSD
2, 1405–1431, 2014

organic matter after the development of seedlings and dwarf shrubs in the SB area. Soil properties in the study area are reported in detail by Ceaglio et al. (2012). As visible in Fig. 2, several erosion evidences were observed such as sheet erosion, particle redeposition after snowmelt in undisturbed sites (not included in this study), removal of vegetation cover in the avalanche release and track areas.

2.3 ^{137}Cs-derived soil redistribution

A Li-drifted Ge detector with a 20 % relative efficiency (GeLi; Princeton Gamma-Tech, Princeton, NJ, USA) was used for gamma spectroscopy. The resulting measurement uncertainty on ^{137}Cs peak area (at 662 keV) was lower than 8 % (error of the measurement at 1-sigma). Gamma spectrometry calibration and quality control were performed following the protocol proposed by Shakhashiro and Mabit (2009). The methods and instruments used are detailed in Ceaglio et al. (2012). Soil samples were collected during summer season 2010, using a 72 mm diameter soil core sampler (Giddings Machine Company, Windsor, CO, USA). ^{137}Cs activity was measured at eleven points in the three subareas: (a) snow bridge (SB), release area (RA), and track areas (TA) (Fig. 1). For the reference inventories eleven points located very close to the study area in a flat and undisturbed position (2000 m a.s.l.) were sampled. Depth distribution of ^{137}Cs was determined in 5 cm depth increments. To convert inventories into soil redistribution rates the profile distribution model, which is the most commonly used conversion model for unploughed soils was used (Walling & Quine., 1990). In undisturbed soils the ^{137}Cs distribution shows an exponential decrease with depth, which is described by the following function (Walling and Quine, 1990; Zhang et al., 1990):

$$A'(x) = A_{\mathrm{ref}}(1 - e^{x/h_o}) \quad (1)$$

where: $A'(x)$ = amount of ^{137}Cs above the depth x (Bq m^{-2})

x = depth from soil surface expressed as mass between top and actual depth (kg m^{-2})

NHESSD
2, 1405–1431, 2014

A_{ref} = ^{137}Cs reference inventory (Bq m^{-2})

h_o = profile shape factor (kg m^{-2}), it is a coefficient describing the rate of exponential decrease in inventory with depth, for soil profiles in u sites.

If it is assumed that the total ^{137}Cs fallout occurred in 1986 and that the depth distribution of the ^{137}Cs in the soil profile is independent of time, the erosion rate Y for an eroding point (total ^{137}Cs inventory A_u (Bq m^{-2}) less than the local reference inventory A_{ref} (Bq m^{-2})) can be expressed as (Walling and Quine, 1990; Zhang et al., 1990):

$$Y = 10/(t - 1986) \cdot \ln(1 - X/100) \cdot h_o \quad (2)$$

where:

Y = soil erosion rate (t ha^{-1} yr^{-1})

t = year of sampling

1986 = because in Valle d'Aosta Region the contribution of Chernobyl wet deposition constituted the major part of the global inventory (84 % according to Facchinelli et al., 2002)

X = % reduction of ^{137}Cs total inventory in respect to the local ^{137}Cs reference value (defined as: $(A_{ref} - A_u)/A_{ref} \times 100$)

2.4 RUSLE-derived soil erosion and Winter factor calculation

The Revised Universal Soil Loss Equation (RUSLE) model is formulated as follows:

$$A = R \cdot K \cdot LS \cdot C \cdot P \quad (3)$$

where:

A = predicted average annual soil loss (t ha^{-1} yr^{-1});

R = rainfall-runoff-erosivity factor (MJ mm ha^{-1} h^{-1} yr^{-1}) that quantifies the effects of raindrop impact and reflects the rate of runoff likely to be associated with the rain (Wischmeier and Smith, 1978);

NHESSD
2, 1405–1431, 2014

K = soil erodibility factor ($t\,h\,h\,MJ^{-1}\,ha^{-1}\,mm^{-1}$) reflects the ease with which the soil is detached by impact of a splash or surface flow;

LS = accounts for the effect of slope length (L) and slope gradient (S) on soil erosion (dimensionless);

C = cover factor (dimensionless), which represents the effects of all interrelated cover and management variables (Renard et al., 1997);

P = (dimensionless) is the support practice factor.

The R, K, LS factors basically determine the erosion volume while the C and P factor are reduction factors ranging between 0 and 1.

RUSLE was applied at the eleven sites (Fig. 1), where also ^{137}Cs estimates were available therefore considering representative points. R was taken from Bazzoffi (2007) tabular values indicating an average of $1238\,MJ\,mm\,ha^{-1}\,h^{-1}\,yr^{-1}$ for the Municipality of Courmayeur, where the study area is located. The adopted value is consistent with the ones reported by Meusburger et al. (2012) for the Swiss Alps and the seasonal values in the erosivity maps produced by JRC for Italy (Grimm et al., 2000).

The K factor ($t\,h\,h\,MJ^{-1}\,ha^{-1}\,mm^{-1}$) was calculated according to Wischmeier and Smith (1978) using the following equation adopted also by Bazzoffi (2007) for Italy:

$$K = 0.0013175 \cdot ((2.1m^{1.14}(10^{-4})(12-a) + 3.25(b-2) + 2.5(c-3)) \quad (4)$$

where m = (silt (%) + very fine sand (%)) × (100 – clay(%)), a = organic matter (%), b = structure code: (1) very structured or particulate, (2) fairly structured, (3) slightly structured and (4) solid and c = profile permeability code: (1) rapid, (2) moderate to rapid, (3) moderate, (4) moderate to slow, (5) slow and (6) very slow. For the determination of the K factor the values of the upper 10 cm of soil were used. Soil samples were oven-dried at 40 °C, passed through a 2 mm sieve and homogenized. The fine material (< 2 mm) was used for all further analysis. Total organic and inorganic carbon concentration (%) was measured by the RC612 Multiphase Carbon and Hydrogen/Moisture Analyzer (Leco company, MI, USA). Organic matter was calculated from organic carbon content by using the conversion factor of 1.72. Grain size analysis for the param-

NHESSD
2, 1405–1431, 2014

eter m was done with the Malvern Mastersizer 2000 (Malvern Instruments Ltd). Here we adopted b equal to 2 and c equal to 3, as soil structure was at all the sampling points fairly developed, due to slope angles and limited soil profile development, and soil permeability was estimated in the field as moderate.

The LS factor (dimensionless) was calculated from the digital elevation model (10 m grid) of the study area according to the procedure described in Desmet and Govers (1996, (see also Bazzoffi, 2007)). We adopted the equation

$$LS = (F \cdot C/22.13)^{0.4} \cdot (\sin S/0.0896)^{1.3} \quad (5)$$

where F is the flow accumulation factor (Mitasova et al., 2002), C is the grid size (here, 10 m), S is the slope angle. F was calculated with the Hydrology tool of ArcGIS 9.3.

The C factor was derived from tabular data proposed by Bazzoffi (2007) for grass and pasture vegetation cover. The P factor was not applicable in the area and was therefore considered equal to 1. RUSLE was run for the points and subareas represented in Fig. 1.

In order to estimate the contribution of winter erosion, we calculated a W-factor as proposed by Konz et al. (2009) and Meusburger et al. (2013), to be added to the RUSLE formula, as the ratio between ^{137}Cs and RUSLE based soil erosion rates (both in t ha^{-1} yr^{-1} and therefore dimensionless):

$$W = {}^{137}\mathrm{Cs}/A. \quad (6)$$

2.5 Avalanche modeling

The dynamical model RAMMS (RApid Mass Movements) – Avalanche module (Christen et al., 2010), developed by the SLF of Davos (CH), was used in order to simulate the effect of the avalanches and in particular to calculate the friction at the flow bottom. RAMMS numerically solves a system of partial differential equations, governing the depth-averaged balance laws for mass, momentum and random kinetic energy using first and second order finite volume techniques. More details on the model are given

NHESSD
2, 1405–1431, 2014

in Christen et al. (2010). In this work, the Voellmy–Salm approach is used, where the total basal friction τ (Pa) is split into a velocity independent dry-Coulomb term which is proportional to the normal stress σ (Pa) at the flow bottom (friction coefficient μ) and a velocity dependent turbulent friction (friction coefficient ξ ($m\,s^{-2}$)) (Salm, 1993):

$$\tau = \mu\,\sigma + \frac{\rho\,g\,U^2}{\xi} \tag{7}$$

where $\sigma = \rho\,g\,H\cos\varphi$ with ρ ($kg\,m^{-3}$) the snow mass density, g the gravity ($m\,s^{-2}$), H (m) the avalanche flow height and ϕ (°) the local slope angle, and U ($m\,s^{-1}$) is the flow velocity.

Soil erosion can occur if the shear stress exerted by the avalanche flow is larger than the critical shear for soil removal τ_c (Pa) calculated as in Clark and Wynn (2007) and later reported by Confortola er al. (2012):

$$\tau_{c,Pc} = 0.49 \times 10^{0.0182\,P_c} \tag{8}$$

where P_c is the clay content.

We simulated an avalanche that is considered typical for the study site: a frequent avalanche (short return period) with the release zone between 2050 and 2100 m a.s.l., release height of 1 m, release volume of 7800 m^3, friction parameters μ and ξ chosen according to Gruber and Bartelt (2007) all along the path ($\mu = 0.26$ and $\xi = 2000\,m\,s^{-2}$ in the sampling points).

We underline here that the aim of the avalanche modeling is not to simulate the real events, but to estimate the erosive power of what can be considered the most representative avalanche for the path. Therefore, the results of the simulation should be interpreted in a relative way for the different sampling points.

NHESSD
2, 1405–1431, 2014

3 Results and discussion

The RUSLE factors at sampled points are listed in Table 1. K-factor values (Table 1), indicating the intrinsic soil susceptibility to water erosion, ranged from 0.005 (sample SB-T1P5, with highest clay content) to 0.030 $t\,ha\,h\,MJ^{-1}\,ha^{-1}\,mm^{-1}$ (sample SB-T1P1, lowest organic matter content). The observed range is comparable with the mapped values reported for Aosta Valley by Grimm et al. (2000). Highest erodibility was observed in the upper part of the transect of SB and RA (Fig. 3). The C-factor (Table 1) was assigned a value of 0.02 in the SB area with dwarf shrubs and seedlings cover and of 0.005 in RA and TA. LS-factor at sampling points (Table 1) ranged from 3 to 37 (both observed in TA). High LS values are largely documented in literature for non-agricultural environments. For example, Meusburger et al. (2010) reported LS values in the range 0–57.5 for a study site in the Swiss Alps with an average slope of 24.6°. LS in the whole area (Fig. 3) ranged from values close to 0 to values exceeding 50 (TA, highly channeled with steep, complex slopes), and the slope angle varied in the range 29–46° (Table 1). The slope interval confirms that the area is potentially prone to both snow gliding (Leitinger et al., 2008) and snow-glide avalanches (Confortola et al., 2012). RUSLE factors K and LS did not differ significantly among subareas.

RUSLE soil erosion rates at the sampled sites (Table 2) ranged from close to 0 (TA-T14 and TA-T21) to 17 $t\,ha^{-1}\,yr^{-1}$ (SB-T1P1, upper part of the SB area). Such values refer to the first three erosion risk classes reported by Bazzoffi (2007), i.e. negligible ($< 1\,t\,ha^{-1}\,yr^{-1}$), limited ($1 < A < 5\,t\,ha^{-1}\,yr^{-1}$), and moderate ($5 < A < 20\,t\,ha^{-1}\,yr^{-1}$).

Average RUSLE estimates were 13.2 $t\,ha^{-1}\,yr^{-1}$ for SB (st. dev. 7.0), 1.9 $t\,ha^{-1}\,yr^{-1}$ for TA (st. dev. 1.9), and 2.2 $t\,ha^{-1}\,yr^{-1}$ for RA (st. dev. 1.4). The RUSLE estimates were significantly higher in SB than in the rest of the area ($p < 0.01$). The range (Table 2) of ^{137}Cs estimates was −0.1 to 32 $t\,ha^{-1}\,yr^{-1}$, where the negative value observed in SB-T1P5 indicates a net deposition rate. Average ^{137}Cs values were 13.2 $t\,ha^{-1}\,yr^{-1}$ for SB (st. dev. 15.4), 11.6 for TA (st. dev. 11.8), and 9.1 for RA (st. dev. 4.8). High spatial heterogeneity was observed for the ^{137}Cs erosion rates particularly in TA and

NHESSD
2, 1405–1431, 2014

SB (Table 2), and this made the observed differences not statistically significant. In TA, high variability in ^{137}Cs estimates probably depended on the high variability of soil characteristics, as visible also from the *K* values and the channeled topography (Fig. 3). The variability of the ^{137}Cs erosion rates in the SB area may be instead attributed to the simultaneous presence of erosion and deposition dynamics.

In fact, the ^{137}Cs erosion rates confirmed the importance of soil erosion in the upper portion of the SB area (Table 2) with 30 t ha^{-1} yr^{-1} (SB-T1P1), while a sharp reduction of the net erosion rates was visible downwards, along the snow bridge structures. At point SB-T1P3 the ^{137}Cs erosion rate dropped to 10 t ha^{-1} yr^{-1}, and deposition was finally observed at point SB-T1P5 (Table 2) indicating a net input of topsoil that was also associated to an increase in soil organic matter downwards. This can be interpreted as the result of a positive action of snow bridges as defence structure mitigating slow snow movements, thus reducing drastically winter erosion rates. Also RUSLE based soil erosion rates (A, Table 2) showed a decreasing trend downslope in SB, but in this case the reduction was smoother and followed the decrease in erodibility values visible from Fig. 3: 0.030 t ha h MJ^{-1} ha^{-1} mm^{-1} (SB-T1P1, 4.9 % organic matter) to 0.026 t ha h MJ^{-1} ha^{-1} mm^{-1} (SB-T1P3, 5.6 % organic matter), and finally 0.005 t ha h MJ^{-1} ha^{-1} mm^{-1} (SB-T1P5, 12 % organic matter). It has to be noticed that in the SB area LS was almost constant. Therefore, a direct effect of the topographic factor on the deposition processes can be excluded. The protection of the avalanche defence structures against soil erosion, slowing down the snow movements in winter, allowed over time the colonization by shrubs and larch seedlings that can locally reduce soil erosion in the vegetative season. The following chain effects can be hypothesised with time: physical barriers determine a reduction of snow gliding i.e. less soil erosion; natural regeneration is favored, natural renovation enhances the protection against erosion; soil organic matter increases; soil erodibility decreases; soil erosion is again reduced.

In general, ^{137}Cs estimates gave higher erosion rates at sampled points than the potential erosion estimates obtained with RUSLE (Table 2). The discrepancies between

NHESSD
2, 1405–1431, 2014

^{137}Cs and RUSLE erosion rates obtained in our study (Table 2) are consistent with the ones shown in Konz et al. (2009), who found that ^{137}Cs erosion rates ranged between 5 and 37 $t\,ha^{-1}\,yr^{-1}$, while USLE estimates did not exceed 15 $t\,ha^{-1}\,yr^{-1}$. When the dataset is studied as a whole, no significant correlation is visible between the two variables (r = 0.486, ns), and an outlier represented by point TA-T25 is clearly evident. Disregarding the outlier, the correlation improves considerably (r = 0.622, p = 0.055, at the limit of significance). The extreme behavior of point TA-T25 can be easily explained by its LS value (37), the highest in the study area, which can be considered extreme with respect to the remaining points. The differences between estimates do not appear related to the variation of a single RUSLE factor such as topography or erodibility.

We observed that most points characterised by limited water erosion potential ($1 < A < 5\,t\,ha^{-1}\,yr^{-1}$) because of low K and/or LS factors (TA-T12, TA-T14, TA-T21, TA-T23, TA-T25, whole RA), showed ^{137}Cs erosion rates more than twice as high compared to A (only exception, RA-T33 where A and ^{137}Cs estimates were closer). Our hypothesis is that despite the intrinsic soil properties and/or topographic conditions, in these sampling sites the contribution of winter erosion (i.e. avalanche erosion and/or snow gliding) is particularly severe. In fact, literature findings showed that the erosion rates determined by avalanche run can be significant and non-selective, i.e. act independent of soil properties and size classes, but are rather controlled by the depth and velocity of the snow mass (Confortola et al., 2012). This would be applicable to the track area. In RA snow gliding and incipient avalanche movements can be hypothesised, too, and have been documented by Ceaglio et al. (2014) who observed snow glide rates in the order of magnitude of several meters. The SB area, despite a rather homogeneous LS factor (range 20–23), showed sharp differences in erodibility and a reduction trend along slope that was visible for both RUSLE and ^{137}Cs erosion rates, for the latter even a deposition at the bottom of the area estimated (Table 2). The box plot of Fig. 4a depicts the difference obtained subtracting A from ^{137}Cs estimates. This difference represents the relative importance of winter erosion (avalanches + snow gliding + snow melt) with respect to total erosion budget (estimated with ^{137}Cs). The median (black horizon-

NHESSD
2, 1405–1431, 2014

tal line) is similar for TA and RA, while it drops considerably in SB, suggesting different prevailing snow induced processes in the snow bridge area, such as the protection effect carried out by snow bridges against snow gliding. The discrepancy in RA and TA is much less evident, except for one outlier (TA-T25), characterised by an extreme LS value (Table 1).

The proposed W values (dimensionless) are presented for the sampling points in Table 2. W varied from −0.29 (minus sign indicating the deposition section SB-T1P5) to approximately 39 (TA-T21), with considerable spatial variability. The range of values for the three considered subareas fell in the range found by Konz et al. (2009), which varied from 0.4–17.5 for an mountain environment in Switzerland, where the main snow induced disturbance was snow gliding.

The box plot in Fig. 4b shows the W distribution in the three subareas. It is clearly visible that the SB area has a median W value less than < 2 On the contrary, TA and RA show similar median values in the range 5–10, with extreme cases where W exceeds 20, and denote some role of winter erosion processes. In TA the dispersion of the W frequency distribution was higher, and likely related to the high terrain variability and complex morphology.

We are conscious of the limited number of areas studied, but the pattern observed in the W factor distribution suggest that the differences between erosion estimates can be linked to the prevailing winter dynamics, i.e. the SB area, RA, TA have a different behavior because the acting forces vary.

In order to reinforce this interpretation, the avalanche model RAMMS was applied.

The results, extracted for the sampling points considered for W estimation, are presented in Table 3. Points in the release area are not presented because the model performance is not optimal at the very beginning of the avalanche track. The snow bridge area is obviously excluded as it is not affected by avalanches.

Points TA-T12 and TA-T14 (see Fig. 3 and Table 3) show the lowest values of normal (σ) and shear (τ) stress as they are located at the side of the avalanche track, where the flow height (H) and velocity (U) are lower than in the middle of the track, while the

NHESSD
2, 1405–1431, 2014

remaining points (TA-T21, TA-T23, and TA-T25) are along a transect in middle of the avalanche path, where avalanche bottom shear stresses increased considerably.

The shear stress exerted by the avalanche increased with the avalanche velocity and height. The critical shear stress τ_c calculated for soil according to the formula proposed by Clark and Wynn (2007) was in the range of values reported by Confortola et al. (2012) and at least two orders of magnitude lower than the stress exerted by the avalanche (Table 3). Therefore, the model generally confirmed that the avalanche action actually produces erosive effects on the soil surface.

However, no clear relationship between *W* and avalanche modeled parameters could be observed. This could depend on (a) the small number of points (only 5) that could be considered in the comparison between *W* and the avalanche modeled parameters and (b) the impossibility to assess the relative weight of snow gliding and avalanche erosion rates with the available data. The latter statement is particularly true for points TA-T12 and TA-T14, close to the boundary, where different winter processes, characterised by different intensities, can coexist.

The findings of the present research in terms of *W* order of magnitude, ranges and patterns seem promising; however, further validation with a larger dataset and with punctual measurement of snow gliding rates will be needed to establish the appropriate basis for an adaption of the RUSLE to alpine environments.

4 Conclusions

The application of RUSLE in a study site in the Italian Western Alps prone to snow gliding and glide-snow avalanches was compared with ^{137}Cs method estimates. In general, the ^{137}Cs estimates, which intergrate all erosion processes, were higher than RUSLE estimates that only consider water induced soil erosion (i.e. erosion taking place on snow-free soil). Three subareas were considered: RA, release area, interested by avalanche detachment and potential snow gliding; TA, track area, affected by the avalanche run; SB, snow bridge area, potentially influenced by snow-gliding only.

NHESSD
2, 1405–1431, 2014

The obtained RUSLE erodibility parameters (K) and ^{137}Cs estimates evidenced an effective erosion mitigation by the snow bridges, that progressively stopped the gliding movements acting as a physical barrier.

The RUSLE estimates and the ^{137}Cs redistribution gave significantly different results. ^{137}Cs-based erosion rates were generally higher and therefore suggested the introduction of a winter correction factor (W – dimensionless) for RUSLE, taking into account winter erosion processes, besides the water erosion taking place during the vegetative period.

W ranges evidenced some relevant differences in the role of winter erosion in the considered subareas. In fact, the SB area showed lover W values (< 2), TA and RA showed similar median values (in the range 5–10) with extreme cases where W exceeded 20. The application of the RAMMS avalanche simulation model corroborated these findings.

Despite the limited sample size (11 points) the inclusion of a W factor into RUSLE seems promising for the improvement of soil erosion estimates in Alpine environments affected by snow movements.

Acknowledgements. This research was supported by the Italian MIUR Project (PRIN 2010-11): "Response of morphoclimatic system dynamics to global changes and related geomorphological hazards" (national coordinator C. Baroni). We would like to thank also the Ufficio Centro Funzionale (Regione Autonoma Valle d'Aosta - Assessorato opere pubbliche, difesa del suolo e edilizia residenziale pubblica – Dipartimento difesa del suolo e risorse idriche) for datasets, and the WSL-SLF of Davos (CH) for the use of RAMMS.

References

Alewell, C., Meusburger, K., Brodbeck, M., and Bänninger, D.: Methods to describe and predict soil erosion in mountain regions, Landscape Urban Plan., 88, 46–53, 2008.

Bazzoffi, P.: Erosione del Suolo e Sviluppo Rurale, Edagricole, Bologna, 249 pp., 2007.

NHESSD

2, 1405–1431, 2014

Ceaglio, E., Meusburger, K., Freppaz, M., Zanini, E., and Alewell, C.: Estimation of soil redistribution rates due to snow cover related processes in a mountainous area (Valle d'Aosta, NW Italy), Hydrol. Earth Syst. Sci., 16, 517–528, doi:10.5194/hess-16-517-2012, 2012.

Ceaglio, E., Freppaz, M., Filippa, G.,Ferraris, S., Segor, V., and Zanini, E.: Snow gliding processes and predisposing factors in a glide-snow avalanche release area (Valle d'Aosta, NW Italian Alps), CRST, submitted, 2014.

Christen, M., Kowalski, J., and Bartelt, P.: RAMMS: numerical simulation of dense snow avalanches in three-dimensional terrain, Cold Reg. Sci. Technol., 63, 1–14, 2010.

Clark, L. A. and Wynn, T. M.: Methods for determining streambank critical shear stress and soil erodibility: implications for erosion rate predictions, American Society of Agricultural and Biological Engineers, 50, 95–106, 2007.

Confortola, G., Maggioni, M., Freppaz, M., and Bocchiola, D.: Modelling soil removal from snow avalanches: a case study in the Italian Alps, Cold Reg. Sci. Technol., 70, 43–52, 2012.

Desmet, P. J. J. and Govers, G.: A GIS procedure for automatically calculating the USLE LS factor on topographically complex landscapes units, J. Soil Water Conserv., 51, 427–433, 1996.

Facchinelli, A., Magnini, M., Gallini, L., and Bonifacio, E.: ^{137}Cs contamination from Chernobyl of soils in Piemonte (North-West Italy): spatial distribution and deposition model, Water Air Soil Poll., 134, 341–352, 2002.

Freppaz, M., Lunardi, S., Maggioni, M., Valfré, F., Bizzocchi, T., and Zanini, E.: Soil erosion caused by snow avalanches: preliminary results of two case studies in the Aosta Valley (NWItaly), in: Proceeding of the International Snow Science Workshop: a Merging between Theory and Practice (ISSW 2006) Telluride, Colorado, USA, 1–7 October 2006, 880–886, 2006.

Freppaz, M., Godone, G., Filippa, G., Maggioni, M., Lunardi, S., Williams, M. W., and Zanini, E.: Soil erosion caused by snow avalanches: a case study in the Aosta Valley (NW Italy), Arct. Antarct. Alp. Res., 42, 4, 412–421, 2010.

Grimm, M., Jones, R. J. A., Rusco, E., and Montanarella, L.: Soil Erosion Risk in Italy: a revised USLE approach, European Soil Bureau Research Report No.11, EUR20677 EN, (2002), 28 pp. Office for Official Publications of the European Communities, Luxembourg, 2003.

Gruber, U. and Bartelt, P.: Snow avalanche hazard modelling of large areas using shallow water numerical methods and GIS, Environ. Modell. Softw., 22, 1472–1481, 2007.

NHESSD
2, 1405–1431, 2014

Joint Research Center Ispra: Nature and extent of soil erosion in Europe, Commission European Communities, http://ec.europa.eu/environment/soil/pdf/vol2.pdf, (accessed date: 28/1/14)), 2009a.
Joint Research Center Ispra: Soil erosion in the Alps (RUSLE) http://eusoils.jrc.ec.europa.eu/library/Themes/Erosion/ClimChalp/Rusle.html (last access: 7January 2009), 2009b.
Konz, N., Schaub, M., Prasuhn, V., Baenninger, D., and Alewell, C.: Cesium-137-based erosion-rate determination of a steep mountainous region, J. Plant Nutr. Soil Sc., 172, 615–622, 2009.
Konz, N., Prasuhn, V., and Alewell, C.: On the measurement of Alpine soil erosion, Catena, 91, 63–71, 2012.
Lal, R.: Soil degradation by erosion, Land Degr. Develop., 12, 519–539, 2001.
Leitinger, G., Höller, P., Tasser, E., Walde, J., and Tappeiner, U.: Development and validation of a spatial snow-glide model, Ecol. Model., 211, 363–374, 2008.
Mabit, L. and Bernard, C.: Assessment of spatial distribution of fallout radionuclides through geostatistics concept, J. Environ. Radioactiv., 97, 206–219, 2007.
Mabit, L., Benmansour, M., and Walling, D. E.: Comparative advantages and limitations of the fallout radionuclides ^{137}Cs, ^{210}Pb(ex) and ^{7}Be for assessing soil erosion and sedimentation, J. Environ. Radioactiv., 99, 1700–1807, 2008.
Mabit, L., Meusburger, K., Fulajtar, E., and Alewell, C.: The usefulness of ^{137}Cs as a tracer for soil erosion assessment: a critical reply to Parsons and Foster (2011), Earth-Sci. Rev., 127, 300–307, 2013.
Matisoff, G. and Whiting, P. J.: Measuring Soil Erosion Rates Using Natural (Be-7, Pb-210) and Anthropogenic (Cs-137, Pu-239,Pu-240) Radionuclides, Handbook of Environmental Isotope Geochemistry, Vols 1 and 2, edited by: Baskaran, M., Springer-Verlag Berlin, Berlin, 487–519, 2011.
Meusburger, K., Konz, N., Schaub, M., and Alewell, C.: Soil erosion modelled with USLE and PESERA using QuickBird derived vegetation parameters in an Alpine catchment, Int. J. Appl. Earth Obs., 12, 208–215, 2010.
Meusburger, K., Steel, A., Panagos, P., Montanarella, L., and Alewell, C.: Spatial and temporal variability of rainfall erosivity factor for Switzerland, Hydrol. Earth Syst. Sci., 16, 167–177, doi:10.5194/hess-16-167-2012, 2012.
Mitasova, H., Mitas, L., and Brown, W. M.: Multiscale simulation of land use impact on soil erosion and deposition patterns, in: Sustaining the Global Farm, Selected papers from the

NHESSD
2, 1405–1431, 2014

10th ISCO Meeting held 24–29 May 1999 at Purdue University and the USDA-ARS NSERL, edited by: Stott, D. E., Mohtar, R. H., and Steinhart, G. C., 1163–1169, 2002.
Prasuhn, V., Linniger, H., Gisler, S., Herweg, K., Candinas, A., and Clement, J. P.: A high-resolution soil erosion risk map of Switzerland as strategic policy support system, Land Use Pol., 32, 281–291, 2013.
Renard, K., Foster, G., Weesies, G., McCool, D., and Yoder, D.: Predicting soil erosion by water: a guide to conservation planning with the Revised Universal Soil Loss Equation (RUSLE), USDA Agriculture Handbook #703, 384 pp., 1997.
Ritchie, J. C. and McHenry, J. R.: Application of radioactive fallout cesium-137 for measuring soil-erosion and sediment accumulation rates and patterns – a review, J. Environ. Qual., 19, 215–233, 1990.
Salm, B.: Flow, flow transition and runout distances of flowing avalanches, Ann. Glaciol., 18, 221–226, 1993.
Shakhashiro, A. and Mabit, L.: Results of an IAEA inter-comparison exercise to assess ^{137}Cs and total ^{210}Pb analytical performance in soil, Appl. Radiat. Isot., 67, 139–46, 2009.
Tamura, T.: Selective sorption reaction of caesium with mineral soils, Nucl. Safety, 5, 262–268, 1964.
Tamura, T. and Jacobs, D. G.: Structural implications in cesium sorption, Health Phys., 2, 391–398, 1960.
US Department of Agriculture, S. C. S.: Procedure for Computing Sheet and Rill Erosion on Project Areas. Soil Conservation Service, Technical Release No. 51 (Rev. 2)., 1977.
Walling, D. E. and Quine., T. A.: Calibration of caesium-137 measurements to provide quantitative erosion rate data, Land Degrad. Rehabil., 2, 161–173, 1990.
Wischmeier, W. H. and Smith, D. D.: Predicting Rainfall Erosion Losses – A Guide to Conservation Planning, Agric. Handbook No. 537, Washington, DC, 1978.
Zhang, H., Yang, Q., Rui, L., Liu, Q., Moore, D., He, P., Ritsema, C. J., and Geissen., V.: Extension of a GIS procedure for calculating the RUSLE equation LS factor, Comput. Geosci., 52, 177–188, 2013.

NHESSD
2, 1405–1431, 2014

Table 1. RUSLE factors inputs, results and slope angle at the studied sampled points.

Sample ID	Soil Depth (cm)	Fine sand (%)	Silt (%)	Clay (%)	SOM (%)	K (t ha h MJ^{-1} mm^{-1} ha^{-1})	R (MJ mm ha^{-1} h^{-1} yr^{-1})	LS factor (–)	Slope (°)	C factor (–)
SB-T1P1	0–10	5.35	48.7	12.7	4.9	0.030	1238	22.56	36	0.02
SB-T1P3	0–10	7.4	45.0	13.0	5.6	0.026	1238	20.48	32	0.02
SB-T1P5	0–10	6.5	46.9	16.6	12.0	0.005	1238	22.76	37	0.02
TA-T12	0–10	7.06	39.7	8.8	7.2	0.018	1238	11.92	46	0.005
TA-T14	0–10	6.4	47.9	12.6	8.7	0.014	1238	3.55	37	0.005
TA-T21	0–10	9.3	47.3	12.2	9.4	0.012	1238	3.79	29	0.005
TA-T23	0–10	8.0	44.6	10.9	6.7	0.022	1238	17.01	37	0.005
TA-T25	0–10	7.3	49.9	13.9	7.1	0.022	1238	37.00	37	0.005
RA-T31	0–10	6.9	41.6	10.1	5.1	0.027	1238	9.03	37	0.005
RA-T33	0–10	5.9	46.0	12.9	7.9	0.017	1238	36.42	36	0.005
RA T34	0–10	4.9	45.2	15.2	9.4	0.010	1238	21.11	29	0.005

NHESSD
2, 1405–1431, 2014

Table 2. ^{137}Cs and RUSLE estimates, and corresponding calculated W (winter factor). Negative values correspond to sedimentation rates.

Sample ID	Altitude (m a.s.l.)	A ($t\,ha^{-1}\,yr^{-1}$)	$_{137}$Cs ($t\,ha^{-1}\,yr^{-1}$)	W
SB-T1P1	2085	16.73	30.01	1.79
SB-T1P3	2078	13.33	10.02	0.75
SB-T1P5	2060	2.72	−0.29	−0.10
TA-T12	1977	1.34	2.42	1.81
TA-T14	2001	0.31	7.43	23.76
TA-T21	1956	0.28	10.7	38.54
TA-T23	1989	2.36	5.58	2.36
TA-T25	2016	5.07	32.06	6.32
RA-T31	2099	1.49	13.77	9.21
RA-T33	2084	3.75	4.19	1.12
RA T34	2070	1.29	9.37	7.25

NHESSD
2, 1405–1431, 2014

Table 3. Output of the avalanche model RAMMS at sampled points (H flow height, U velocity, σ normal stress, τ basal shear stress) and T_c the critical soil shear stress.

Sample ID	H (m)	U ($m\,s^{-1}$)	σ (Pa)	τ (Pa)	T_c (Pa)
TA-T12	0.16	10.9	401.1	278.9	1.42
TA-T14	0.24	14.9	563.51	472.9	1.66
TA-T21	1.02	20.4	2545.9	1273.7	1.63
TA-T23	1.03	20.7	2396.1	1252.8	1.55
TA-T25	1.23	19.8	2987.3	1353.0	1.76

NHESSD
2, 1405–1431, 2014

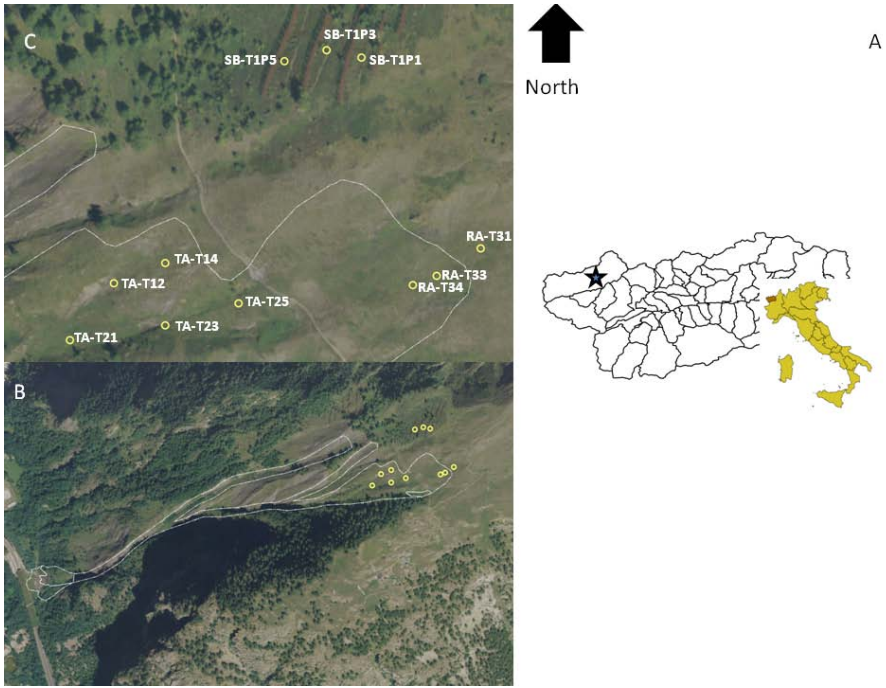

Fig. 1. Study area: **(A)** site location (star) within Italy and the Valle d'Aosta Region; **(B)** avalanche area and sampling points and **(C)** sampling points in detail.

NHESSD
2, 1405–1431, 2014

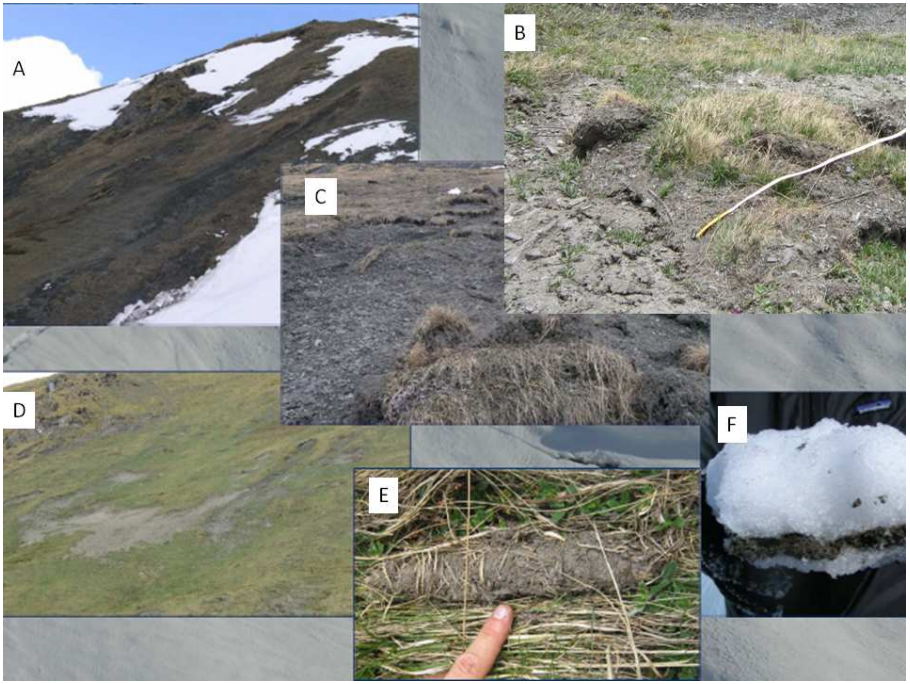

Fig. 2. Evidence of erosion features in the avalanche release area. **(A)** view of the avalanche release area just after the snow melt (RA); **(B)** shallow landslide occurred in winter time, under snow cover, probably as a consequence of snow glide movements; **(C)** zoom on soil erosion and shallow landslides in RA; **(D)** view of eroded surface in the summer season; **(E)** soil "roll" including vegetation residuals, visible after snowmelt, probably due to snow gliding; **(F)** soil layer included in the snow bottom layer during spring time (photos: E. Ceaglio). Soil can undergo liquefaction processes when the soil water content increases. This may result in the layer found at the bottom of the snow pack observed in Fig. 2f.

NHESSD
2, 1405–1431, 2014

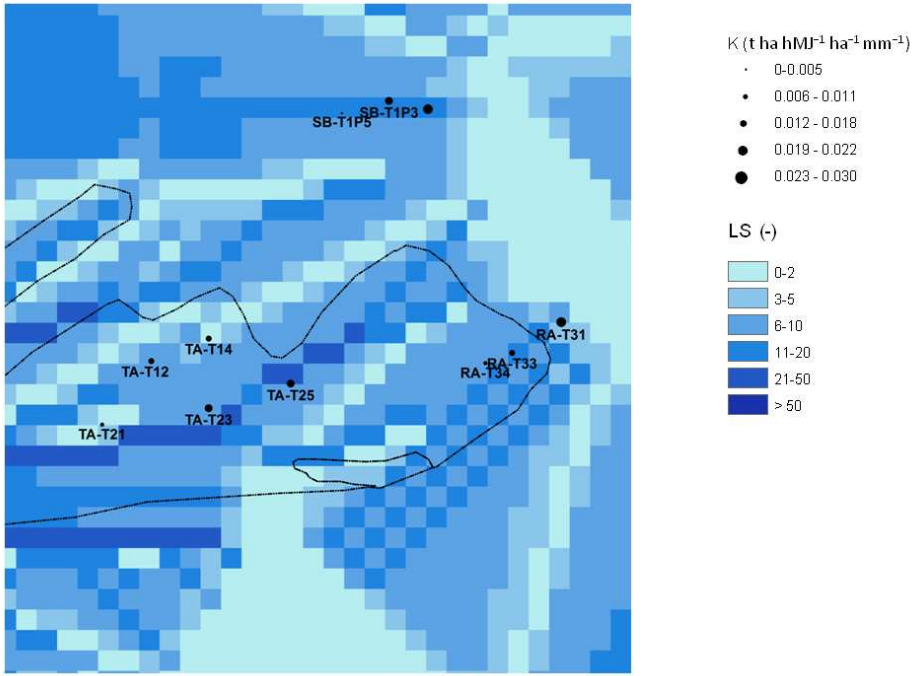

Fig. 3. LS factor map. The sampling point size is proportional to soil erodibility (K) values.

NHESSD
2, 1405–1431, 2014

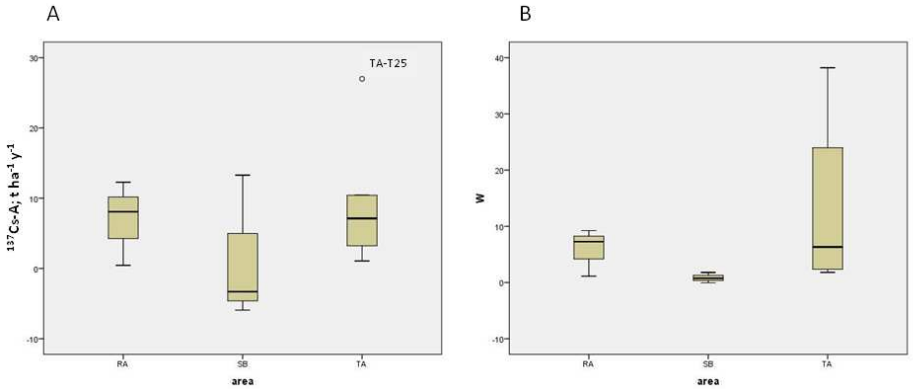

Fig. 4. (A) Difference between ^{137}Cs and RUSLE estimates (^{137}Cs-*A*; t ha^{-1} yr^{-1}) **(B)** and *W* values (–) for the three different subareas (RA = release area, SB = snow bridge area, TA = track area).

NHESSD
2, 1405–1431, 2014